Search for Supersymmetry with Gauge-Mediated Breaking in Diphoton Events with Missing Transverse Energy at CDF II

(Dated: December 8, 2009)

We present the results of a search for supersymmetry with gauge-mediated breaking and $\widetilde{\chi}_1^0 \to \gamma\widetilde{G}$ in the $\gamma\gamma$+missing transverse energy final state. In 2.6±0.2 fb^{-1} of $p\bar{p}$ collisions at $\sqrt{s}$=1.96 TeV recorded by the CDF II detector we observe no candidate events, consistent with a standard model background expectation of 1.4±0.4 events. We set limits on the cross section at the 95% C.L. and place the world's best limit of 149 GeV/c^2 on the $\widetilde{\chi}_1^0$ mass at $\tau_{\tilde{\chi}_1^0} \ll 1$ ns. We also exclude regions in the $\widetilde{\chi}_1^0$ mass-lifetime plane for $\tau_{\tilde{\chi}_1^0} \lesssim 2$ ns.

PACS numbers: 13.85.Rm, 12.60.Jv, 13.85.Qk, 14.80.Ly

The standard model (SM) of elementary particles has been enormously successful, but is incomplete. Theoretical motivations [1] and the observation of the '$ee\gamma\gamma$+missing transverse energy ($\not\!\!E_{\rm T}$)' [2, 3] candidate event by the CDF experiment during Run I at the Fermilab Tevatron provide a compelling rationale to search for the production and decay of new heavy particles that produce events with final state photons and $\not\!\!E_{\rm T}$ in collider experiments. Of particular theoretical interest are supersymmetry (SUSY) models with gauge-mediated SUSY-breaking (GMSB) [1]. These models solve the "naturalness problem" [4] and provide a low-mass dark matter candidate that is both consistent with inflation and astronomical observations [5]. Since many versions of these models have a similar phenomenology, we consider a scenario in which the lightest neutralino ($\tilde{\chi}_1^0$) decays almost exclusively (>96%) into a photon (γ) and a weakly interacting, stable gravitino ($\tilde{G}$). The $\tilde{G}$ gives rise to $\not\!\!E_{\rm T}$ by leaving the detector without depositing any energy [6]. In these models, the $\widetilde{\chi}_1^0$ is favored to have a lifetime on the order of a nanosecond, and the $\tilde{G}$ is a warm dark matter candidate with a mass in the range $0.5 < m_{\tilde{G}} < 1.5$ keV/c^2 [7]. Other direct searches [8–10] have constrained the mass of the $\tilde{\chi}_1^0$ to be greater than 100 GeV/c^2 for various points in parameter space. At the Tevatron sparticle production is predicted to result primarily into gaugino pairs, and the $\widetilde{\chi}_1^0$ mass ($m_{\tilde{\chi}_1^0}$) and lifetime ($\tau_{\tilde{\chi}_1^0}$) are the two most important parameters in determining the final states and their kinematics [1]. Different search strategies are required for $\widetilde{\chi}_1^0$ lifetimes above and below about a nanosecond [11].

This Letter describes a search for GMSB in which gaugino pairs are produced and quickly decay to the $\gamma\gamma+\not\!\!E_{\rm T}+X$ final state, where X denotes other high-$E_{\rm T}$ final state particles [12]. We use a dataset corresponding to an integrated luminosity of 2.6±0.2 fb^{-1} of $p\bar{p}$ collisions collected with the CDF II detector [13] at $\sqrt{s}$=1.96 TeV. This dataset is ten times larger than the one used in our previous search [8]. For the first time in this channel we use a new photon timing system [14] and a new model of the $\not\!\!E_{\rm T}$ resolution (METMODEL) [15]. These additions significantly improve our rejection of backgrounds from instrumental and non-collision sources, which allows us to considerably enhance the sensitivity of the search for large $\widetilde{\chi}_1^0$ masses compared to other Tevatron searches [9]. We also extend the search by addressing $\widetilde{\chi}_1^0$ lifetimes up to 2 ns, which are favored for larger $m_{\tilde{\chi}_1^0}$.

Here we briefly describe the aspects of the detector [13] relevant to this analysis. The magnetic spectrometer consists of tracking devices that measures the z position and time of the $p\bar{p}$ interaction, and the momenta of charged particles inside a superconducting solenoid magnet. The calorimeter consists of electromagnetic (EM) and hadronic (HAD) compartments and is divided into a central part that surrounds the solenoid coil ($|\eta|<1.1$) [2] and a pair of end-plugs that cover the region $1.1<|\eta|<3.6$. The calorimeters are used to identify and measure the 4-momenta of photons, electrons, and jets (j) [16] and to provide $\not\!\!E_{\rm T}$ information. The EM calorimeter is instrumented with a timing system (EMTiming) [14] that measures the arrival time of photons.

Our analysis begins with diphoton events passing the CDF three-level trigger. The combined trigger selection efficiency is effectively 100% if both photons have $|\eta|<1.1$ and $E_{\rm T}>13$ GeV [12, 15]. Offline, both photons are required to be in the fiducial part of the calorimeter and to pass the standard CDF photon identification and isolation requirements [8], with two minor modifications to remove instrumental and electron backgrounds [15, 17]. The remaining events are dominated by SM production of $\gamma\gamma$, γj with $j \to \gamma_{fake}$, and $jj \to \gamma_{fake}\gamma_{fake}$, where γ_{fake} is any object misidentified as a photon. To minimize the number of these events with large $\not\!\!E_{\rm T}$ due to calorimeter energy mismeasurements, we remove events where the azimuthal angle between the $\not\!\!E_{\rm T}$ and the second-highest $E_{\rm T}$ photon is $|\Delta\phi|<0.3$ or if any jet points to an uninstrumented region of the calorimeter [15]. We require a primary collision vertex position with $|z_{\rm vertex}|<60$ cm in order to reduce non-collision backgrounds and to maintain the projective nature of the photon reconstruction in the calorimeter. For events with multiple reconstructed vertices we recalculate the $E_{\rm T}$ of both photons and $\not\!\!E_{\rm T}$ values if picking a different vertex for them reduces the event $\not\!\!E_{\rm T}$.

Non-collision backgrounds coming from cosmic rays and beam-related effects can produce $\gamma\gamma+\not\!\!E_{\rm T}$ candidates,

and are removed from the inclusive $\gamma\gamma$ sample using a number of techniques. Photon candidates from cosmic rays are not correlated in time with collisions. Therefore, events are removed if the timing of either photon, corrected for average path length (t_γ), indicates a non-collision source [15, 17]. Photon candidates can also be produced by beam-related muons that originate upstream of the detector (from the more intense p beam). These are suppressed using standard beam halo identification requirements [17]. A total of 38,053 inclusive $\gamma\gamma$ candidate events pass all the selection requirements.

Backgrounds to the $\gamma\gamma$+$\not\!\!E_{\rm T}$ final state from SM $\gamma\gamma$/ $\gamma\gamma_{fake}/\gamma_{fake}\gamma_{fake}$ and fake $\not\!\!E_{\rm T}$ arise due to energy mismeasurements in the calorimeter or to event reconstruction pathologies. We use the METMODEL [15] to select events with real and significant $\not\!\!E_{\rm T}$, as part of the optimization, and to predict the contribution of SM backgrounds with fake $\not\!\!E_{\rm T}$ due to normal energy measurement fluctuations. This algorithm considers the clustered (jets) and unclustered energy in the event and calculates the probability for fluctuations in the energy measurement to produce $\not\!\!E_T{}^{fluct}$ equivalent to or larger than the measured $\not\!\!E_{\rm T}$, $P_{\not\!\!E_T{}^{fluct}\geq\not\!\!E_{\rm T}}$. This probability is then used to define a $\not\!\!E_{\rm T}$-significance as $-\log_{10}\left(P_{\not\!\!E_T{}^{fluct}\geq\not\!\!E_{\rm T}}\right)$. Events with true and fake $\not\!\!E_{\rm T}$ of the same value have, on average, different $\not\!\!E_{\rm T}$-significance. We use pseudo-experiments to estimate the expected $\not\!\!E_{\rm T}$-significance distribution for SM events with fake $\not\!\!E_{\rm T}$, and the number of mismeasured events above a given $\not\!\!E_{\rm T}$-significance requirement. The jets and unclustered energy are smeared according to their resolution functions in the event. The systematic uncertainty in the METMODEL is dominated by the uncertainty in the resolution functions.

The METMODEL does not account for reconstruction pathologies in SM events without intrinsic $\not\!\!E_{\rm T}$, such as a wrong choice of the primary interaction vertex or tri-photon events with a lost photon. To obtain the prediction for this background we model SM kinematics and event reconstruction using a $\gamma\gamma$ sample generated with a PYTHIA Monte Carlo (MC) [18] that incorporates a detector simulation [19]. Since the pathologies from γj and jj sources are similar in nature, but not included directly in the simulation, we normalize the sample to the number of events in the inclusive $\gamma\gamma$ data sample. We subtract the expectations for energy mismeasurement fluctuations in the MC to avoid double counting. Uncertainties are dominated by the statistics of the MC sample, but also include the small differences between the measured response of the METMODEL to MC simulation events and real data.

Electroweak production of W and Z bosons which decay to leptons can also produce the $\gamma\gamma$+$\not\!\!E_{\rm T}$ signature where one or more of the photons can be fake, but the $\not\!\!E_{\rm T}$ is due to one or more neutrinos. To estimate the contribution from these backgrounds we use MC simulations

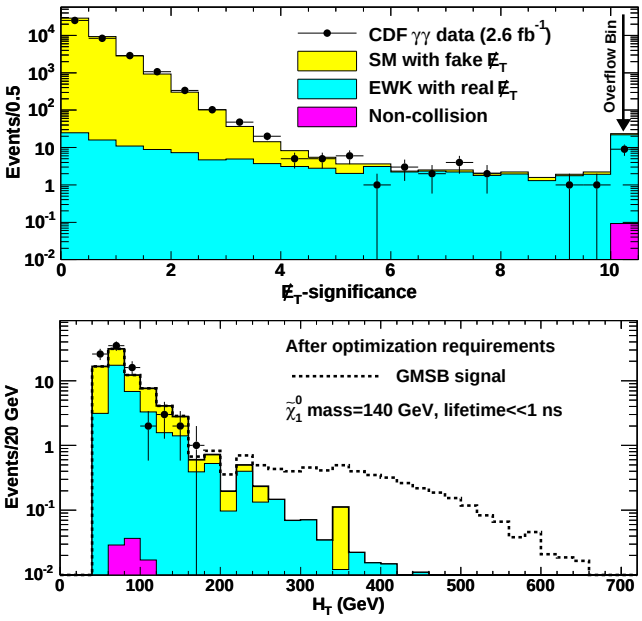

FIG. 1: The top plot shows the $\not\!\!E_{\rm T}$-significance distribution for the inclusive $\gamma\gamma$ candidate sample, along with the background predictions. The bottom plot shows the predicted $H_{\rm T}$ distribution after all but the final $H_{\rm T}$ requirement.

normalized to their theoretical cross sections, taking into account all the leptonic decay modes. The Baur MC [20] is used to simulate $W\gamma$ and $Z\gamma$ production and decay where initial and final state radiation (ISR/FSR) produce W/Z+$\gamma\gamma$ events. The PYTHIA MC is used to simulate backgrounds where both photons are fakes: namely, W and Z, with photons from ISR/FSR removed, and $t\bar{t}$ sources. To minimize the dependence of our predictions on potential "MC-data" differences we scale our MC predictions to the observed number of $e\gamma$ events [15] in data where we use the same diphoton triggers and analysis selection procedures used to select the inclusive $\gamma\gamma$ sample. Uncertainties are dominated by the statistics of the MC and $e\gamma$ normalization data sample.

Non-collision backgrounds are estimated using the data. We identify a cosmic-enhanced sample by using the selected inclusive $\gamma\gamma$ sample, but requiring one of the photons to have t_γ>25 ns. Similarly, we create a beam halo-enhanced sample from events that were filtered out from our signal sample by the beam halo rejection requirements [17]. We estimate the non-collision background events in the signal region using extrapolation techniques and the measured efficiencies of the non-collision rejection requirements [15]. The uncertainties on both non-collision background estimates are dominated by the statistical uncertainty on the number of identified events. Figure 1 (top) shows the $\not\!\!E_{\rm T}$-significance distribution for the inclusive $\gamma\gamma$ sample, along with the predictions for all the backgrounds.

We estimate the sensitivity to heavy, neutral parti-

cles that decay to photons using the GMSB reference model [6] in the mass-lifetime range, $75 \leq m_{\tilde{\chi}_1^0} \leq 150$ GeV and $\tau_{\tilde{\chi}_1^0} \lesssim 2$ ns. Events from all SUSY processes considered [21] are simulated with PYTHIA followed by a detector simulation. The fraction of $\tilde{\chi}_1^0$ decays that occur in the detector volume, and thus the acceptance, depend on both the lifetime and the masses of the sparticles [11]. The total systematic uncertainty on the acceptance, after all kinematic requirements (discussed below), is estimated to be 7%, dominated by the uncertainty in the photon identification efficiency (2.5% per photon). Other significant contributions come from uncertainties on ISR/FSR (4%), jet energy measurement (2%), $\not\!\!E_{\rm T}$-significance parameterizations (1%) and parton distribution functions (PDFs, 1%).

We determine the final kinematic selection requirements by optimizing the mean expected 95% confidence level (C.L.) cross section limit using a no-signal assumption, before looking at the data in the signal region [22]. To compute the predicted cross section upper limit we combine the luminosity, the acceptance, and the background estimates with their systematic uncertainties using a Bayesian method [23]. The predicted limits are optimized by simultaneously varying the selection requirements for $\not\!\!E_{\rm T}$-significance, $H_{\rm T}$ (scalar sum of $E_{\rm T}$ of photons, jets, and $\not\!\!E_{\rm T}$), and the azimuthal angle between the two leading photons, $\Delta\phi(\gamma_1, \gamma_2)$. The large $\not\!\!E_{\rm T}$-significance requirement eliminates most of the SM background with fake $\not\!\!E_{\rm T}$. GMSB production is dominated by heavy gaugino pairs which decay to high-$E_{\rm T}$ light final state particles via cascade decays. The GMSB signal has, on average, larger $H_{\rm T}$ compared to SM backgrounds so that an $H_{\rm T}$ requirement can remove these backgrounds effectively. Electroweak backgrounds with large $H_{\rm T}$ typically consist of a high-$E_{\rm T}$ photon recoiling against $W \to e\nu$, identified as $\gamma_{fake}\not\!\!E_{\rm T}$, which means the gauge boson decay is highly boosted. Thus, the two photon candidates in the final state are mostly back-to-back. The SM backgrounds with fake $\not\!\!E_{\rm T}$ and large H_T also have photons which are mostly back-to-back; the $\Delta\phi(\gamma_1, \gamma_2)$ requirement, therefore, reduces both these backgrounds.

The optimal set of requirements is slightly different for each point in the $\tau_{\tilde{\chi}_1^0}$ vs. $m_{\tilde{\chi}_1^0}$ space considered. We choose a single set of requirements to maximize the region where the predicted production cross section at next-to-leading order [24] is above the expected 95% C.L. cross section limit. The exclusion region also takes into account the production cross section uncertainties, which are dominated by the PDFs (7%) and the renormalization scale (3%). We find the optimal set of requirements, before unblinding the signal region, to be: $\not\!\!E_{\rm T}$-significance>3, $H_{\rm T}>200$ GeV, and $\Delta\phi(\gamma_1, \gamma_2) < \pi - 0.35$. With these requirements we predict 1.4 ± 0.4 background events, 0.9 ± 0.4 of which are from electroweak sources (dominated by $Z\gamma\gamma$ production) with real $\not\!\!E_{\rm T}$, 0.5 ± 0.2 from SM with fake $\not\!\!E_{\rm T}$, and $0.001^{+0.008}_{-0.001}$ from non-collision sources. The acceptance for $m_{\tilde{\chi}_1^0}=140$ GeV/c^2 and $\tau_{\tilde{\chi}_1^0} \ll 1$ ns is estimated to be 7.8 ± 0.6%.

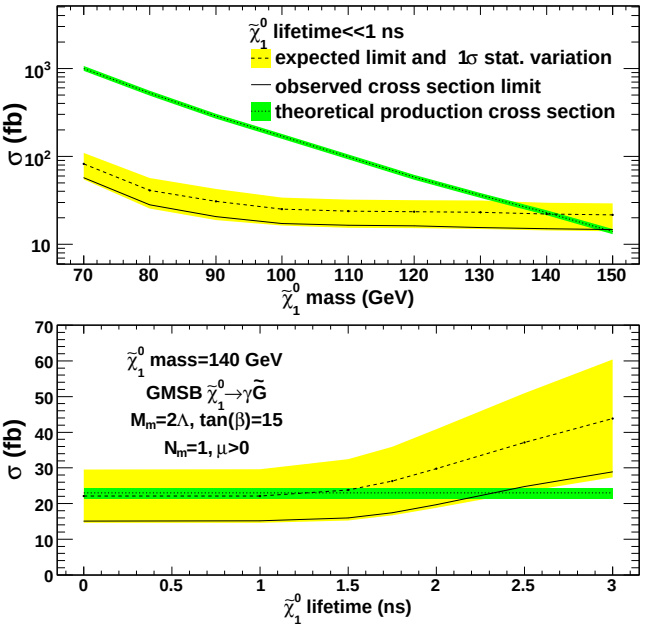

FIG. 2: The predicted and observed 95% C.L. cross section upper limits as a function of the $\tilde{\chi}_1^0$ mass at $\tau_{\tilde{\chi}_1^0} \ll 1$ ns (top) and as a function of the $\tilde{\chi}_1^0$ lifetime at $m_{\tilde{\chi}_1^0}=140$ GeV/c^2 (bottom). Indicated in green (darker shading) is the production cross section, along with its 8.0% uncertainty-band. In yellow (lighter shading) is the RMS variation on the expected cross section limit.

No events in the data pass the final event selection. The predicted $H_{\rm T}$ distribution is shown in Fig. 1 (bottom), after all but the final $H_{\rm T}$ requirement. The data are consistent with the no-signal hypothesis and are well modeled by SM backgrounds alone. We set cross section limits as a function of $m_{\tilde{\chi}_1^0}$ and $\tau_{\tilde{\chi}_1^0}$, respectively, as shown in Fig. 2. The $m_{\tilde{\chi}_1^0}$ reach, based on the predicted and observed number of events for $\tau_{\tilde{\chi}_1^0} \ll 1$ ns, is 141 GeV/c^2 and 149 GeV/c^2 respectively. These limits significantly extend the search sensitivity beyond the results of D0 [9], expand the results to include exclusions for $\tau_{\tilde{\chi}_1^0} \leq 2$ ns, and, when combined with the complementary limits from CDF and LEP [10, 17], cover the region shown in Fig. 3.

In conclusion, we have performed an optimized search for heavy, neutral particles that decay to photons in the $\gamma\gamma + \not\!\!E_{\rm T}$ final state using 2.6 ± 0.2 fb^{-1} of data. There is no excess of events beyond expectations. We set cross section limits using a GMSB model with $\tilde{\chi}_1^0 \to \gamma\tilde{G}$, and find an exclusion region in the $\tau_{\tilde{\chi}_1^0}$-$m_{\tilde{\chi}_1^0}$ plane with the world's best 95% C.L. lower limit on the $\tilde{\chi}_1^0$ mass of 149 GeV/c^2 at $\tau_{\tilde{\chi}_1^0} \ll 1$ ns. By the end of Run II, with an integrated luminosity of 10 fb^{-1}, we estimate a mass

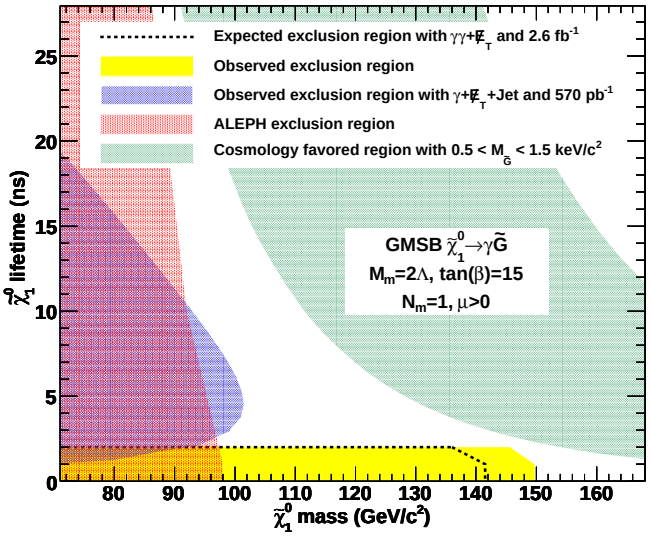

FIG. 3: The predicted and observed exclusion region along with the limits found in [10, 17]. The shaded band shows the parameter space where $0.5<m_{\tilde{G}}<1.5$ keV/c^2, favored by cosmological models [7].

reach of $\simeq 160$ GeV/c^2.

We thank the Fermilab staff and the technical staffs of the participating institutions for their vital contributions. This work was supported by the U.S. Department of Energy and National Science Foundation; the Italian Istituto Nazionale di Fisica Nucleare; the Ministry of Education, Culture, Sports, Science and Technology of Japan; the Natural Sciences and Engineering Research Council of Canada; the National Science Council of the Republic of China; the Swiss National Science Foundation; the A.P. Sloan Foundation; the Bundesministerium für Bildung und Forschung, Germany; the World Class University Program, the National Research Foundation of Korea; the Science and Technology Facilities Council and the Royal Society, UK; the Institut National de Physique Nucleaire et Physique des Particules/CNRS; the Russian Foundation for Basic Research; the Ministerio de Ciencia e Innovación, and Programa Consolider-Ingenio 2010, Spain; the Slovak R&D Agency; and the Academy of Finland.

[1] S. Dimopoulos, S. Thomas, and J. Wells, Nucl. Phys. B **488**, 39 (1997); S. Ambrosanio, G. D. Kribs, and S. P. Martin, Phys. Rev. D **56**, 1761 (1997); G. Giudice and R. Rattazzi, Phys. Rep. **322**, 419 (1999); S. Ambrosanio, G. L. Kane, G. D. Kribs, S. P. Martin, and S. Mrenna, Phys. Rev. D **55**, 1372 (1997).

[2] We use a cylindrical coordinate system in which the proton beam travels along the z-axis, θ is the polar angle, ϕ is the azimuthal angle relative to the horizontal plane, and $\eta=-\ln\tan(\theta/2)$. The transverse energy and momentum are defined as $E_T=E\sin\theta$ and $p_T=p\sin\theta$ where E is the energy measured by the calorimeter and p the momentum measured in the tracking system. $\not{E}_T=|-\sum_i E_T^i \vec{n_i}|$ where $\vec{n_i}$ is a unit vector that points from the interaction vertex to the $i^{\rm th}$ calorimeter tower in the transverse plane.

[3] F. Abe *et al.* (CDF Collaboration), Phys. Rev. Lett. **81**, 1791 (1998) and Phys. Rev. D **59**, 092002 (1999).

[4] S. Martin, arXiv:hep-ph/9709356.

[5] P. Bode, J. Ostriker, and N. Turok, Astrophys. J. **556**, 93 (2001).

[6] B. Allanach *et al.*, Eur. Phys. J. C**25**, 113 (2002). We use benchmark model 8 and take the messenger mass scale $M_{\rm m}$=2Λ, tan(β)=15, $\mu>0$ and the number of messenger fields $N_{\rm m}$=1. The $\tilde{G}$ mass factor and the supersymmetry breaking scale Λ are allowed to vary independently.

[7] C.-H. Chen and J. F. Gunion, Phys. Rev. D **58**, 075005 (1998).

[8] D. Acosta *et al.* (CDF Collaboration), Phys. Rev. D **71**, 031104 (2005).

[9] V. Abazov *et al.* (D0 Collaboration), Phys. Lett. B **659**, 856 (2008).

[10] R. Barate *et al.* (ALEPH Collaboration), Eur. Phys. J. C **28**, 1 (2003); also see M. Gataullin, S. Rosier, L. Xia, and H. Yang, arXiv:hep-ex/0611010; G. Abbiendi *et al.* (OPAL Collaboration), Proc. Sci. HEP2005 346 (2006); J. Abdallah *et al.* (DELPHI Collaboration), Eur. Phys. J. C **38** 395 (2005).

[11] D. Toback and P. Wagner, Phys. Rev. D **70**, 114032 (2004).

[12] E. Lee, Ph.D. thesis, Texas A&M University, 2010.

[13] D. Acosta *et al.* (CDF Collaboration), Phys. Rev. D **71**, 032001 (2005).

[14] M. Goncharov *et al.*, Nucl. Instrum. Methods A**565**, 543 (2006).

[15] T. Aaltonen *et al.* (CDF Collaboration), submitted to Phys. Rev. D, arXiv:0910.5170.

[16] For a discussion of the jet energy measurements, see T. Affolder *et al.* (CDF Collaboration), Phys. Rev. D. **64**, 032001 (2001). For a discussion of standard jet correction systematics, see A. Bhatti *et al.*, Nucl. Instrum. Methods, A **566**, 375 (2006). We use jets with cone size ΔR=0.4.

[17] A. Abulencia *et al.* (CDF Collaboration), Phys. Rev. Lett. **99**, 121801 (2007); T. Aaltonen *et al.* (CDF Collaboration), Phys. Rev. D **78**, 032015 (2008).

[18] T. Sjöstrand *et al.*, Comput. Phys. Commun. **135**, 238 (2001). We use version 6.216.

[19] We use the standard GEANT-based detector simulation [R. Brun *et al.*, CERN-DD/EE/84-1 (1987)] and add a parametrized EMTiming simulation.

[20] U. Baur, T. Han, and J. Ohnemus, Phys. Rev. D **48**, 5140 (1993); U. Baur, T. Han, and J. Ohnemus, *ibid.* **57**, 2823 (1998); The $W\gamma$ and $Z\gamma$ processes are simulated using the leading-order event generator with a k-factor fixed at 1.36. Initial and final state radiation (resulting in additional jets or photons), underlying event, and additional interactions are simulated using PYTHIA [18].

[21] P. Simeon and D. Toback, J. Undergrad. Research in Phys. 20, 1 (2007).

[22] E. Boos, A. Vologdin, D. Toback, and J. Gaspard, Phys. Rev. D **66**, 013011 (2002).

[23] T. Junk, Nucl. Instrum. Methods A**434**, 435 (1999).

[24] We use the leading-order cross sections generated by PYTHIA [18] and the k-factors produced by PROSPINO 2.0 [W. Beenakker *et al.*, Phys. Rev. Lett. **83**, 3780 (1999)].